Gas Sensors Hot Paper

How to cite: *Angew. Chem. Int. Ed.* **2021**, *60*, 19710–19714
International Edition: doi.org/10.1002/anie.202107185
German Edition: doi.org/10.1002/ange.202107185

A Covalent Organic–Inorganic Hybrid Superlattice Covered with Organic Functional Groups for Highly Sensitive and Selective Gas Sensing

*Yingyi Wen[+], Guan-E Wang[+], Xiaoming Jiang, Xiaoliang Ye, Wenhua Li, and Gang Xu**

Abstract: *Organic–inorganic hybrid superlattices (OIHSLs) hold attractive physical and chemical properties, while the construction of single-crystal covalent OIHSLs has not been achieved. Herein a coordination assembly strategy was proposed to create a single-crystal covalent OIHSL PbBDT (BDT = 1,4-benzenedithiolate), where layered [PbS_2] sublattice covalently connects with benzene sublattice. The covalent bonding offers better thermo-/chemi-stability, inter-sublattice electron transport, and unique organic-group-functionalized surface, which may enable better performances in chemical applications than non-covalent OIHSL. These features endow PbBDT with the highest sensitivity, the lowest detection limit and excellent selectivity towards NO_2 at room temperature among all chemiresistive gas-sensing materials with reported response time less than 2 min without the need of light assistance.*

Periodically stacking of two different semiconductor sublattices forms superlattice. The inter-sublattice overlap of electron wavefunctions endows superlattices with exceptional and tunable electronic structures, facilitating their applications in electronics and optoelectronics represented by type-II superlattice photodetectors and quantum cascade lasers.[1] In recent years, organic–inorganic hybrid superlattices (OIHSLs) composed of alternatively overlaid inorganic and organic sublattices have emerged and received enormous attention.[2] Most OIHSLs are easy to fabricate with cheap solution-based methods instead of inefficient and expensive vapor-phase deposition techniques, such as molecular beam epitaxy and metalorganic vapor-phase epitaxy for inorganic superlattices.[3] The incorporation of organic sublattices largely expands the structural diversity of superlattices. Meanwhile, the organic-inorganic synergic effect gives OIHSLs more versatile properties, especially those required for chemistry-involved applications, such as electrocatalysis,[4] energy storage,[5] thermoelectrics,[3a] photocatalysis,[6] and most recently chemical sensing.[7]

To construct semiconductive OIHSLs, a series of synthetic methods have been developed involving either the bottom-up construction of single-crystal superlattice, the intercalation of bulk layered materials, or the reassembly of delaminated layered materials.[2a,c,8] The first strategy produces orderly arranged heterostructures such as IIB-VI and VIIB-VI group hybrid semiconductors [$MQ(L)_x$] (M = Zn, Cd, Mn, et al; Q = S, Se, Te, et al.; L = amines)[9] and layered perovskite ($(RNH_3)BX_4$ (B = Pb, Sn; X = Cl, Br, I).[10] However, in most single-crystal OIHSLs, the connections between organic and inorganic sublattices are weak non-covalent interactions, such as coordination bond, hydrogen bond and electrostatic interactions, which lead to not only inferior thermo-/chemi-stability but also weak inter-sublattice electron coupling.[7b,11] Recently, a series of covalent OIHSLs, metalcone alloys, have emerged with metal oxide nanoslabs interconnected by benzene via covalent bond.[12] Zncone alloy shows good stability and strong electron wavefunction overlap between π-conjugated organic and inorganic sublattices.[13] These features are favorable for chemical applications. However, single-crystal covalent OIHSLs have not been achieved yet. Additionally, metalcone alloys were prepared by inefficient and expensive vapor-phase deposition techniques. Synthetic strategies for the facile preparation of covalent OIHSLs are lacking.

Coordination assembly has been demonstrated an effective way to construct various ordered structures such as metal organic frameworks[14] and coordination polymers.[15] Inspired by that, in this work, a new single-crystal covalent OIHSL, PbBDT (BDT = 1,4-benzenedithiolate), was successfully prepared by high-yield and low-cost solution synthesis. Pb^{2+} and organic thiol were selected as building units to obtain a semiconductive and relatively stable inorganic sublattice. PbBDT has a superlattice structure at atomic precision where the [PbS_2] and benzene sublattices are alternatively connected by S–C covalent bond. Interestingly, a large number of intact benzenethiol groups cover the surface of PbBDT nanosheets. This unique architecture may enhance the electronic change of materials caused by interaction with specific foreign molecules and thus promote their performances in chemical applications. The hypothesis was verified by employing PbBDT nanosheets as NO_2 sensing material, which exhibits the highest sensitivity, the lowest detection

[*] Y. Wen,[+] Dr. G.-E Wang,[+] Dr. X. Jiang, Dr. X. Ye, Dr. W. Li, Prof. G. Xu
State Key Laboratory of Structural Chemistry
Fujian Institute of Research on the Structure of Matter
Chinese Academy of Sciences (CAS)
115 Yangqiao Road West, Fuzhou, Fujian, 350002 (P. R. China)
E-mail: gxu@fjirsm.ac.cn
Y. Wen,[+] Prof. G. Xu
University of Chinese Academy of Sciences (UCAS)
19A Yuquan Road, Beijing 100049 (P. R. China)
Prof. G. Xu
Fujian Science & Technology Innovation Laboratory for Optoelectronic Information of China
Fuzhou, Fujian, 350108 (P. R. China)
[+] These authors contributed equally to this work.
Supporting information and the ORCID identification number(s) for the author(s) of this article can be found under: https://doi.org/10.1002/anie.202107185.

limit, and excellent selectivity among all reported fast-response gas-sensing materials without light assistance.

PbBDT nanosheets were synthesized by one-step coordination assembly of Pb^{2+} ions and 1,4-benzenedithiol under ultrasonic condition (see Supporting Information (SI)). PbBDT single crystal with a suitable size for single-crystal X-ray diffraction was grown by solvothermal method (see SI). PbBDT crystallizes in the monoclinic space group $P2_1/c$ (Table S2), where each Pb atom coordinates with six sulfur atoms from six BDT ligands to constitute a distorted octahedron (Figure 1b). Each [PbS_6] octahedron shares edges with

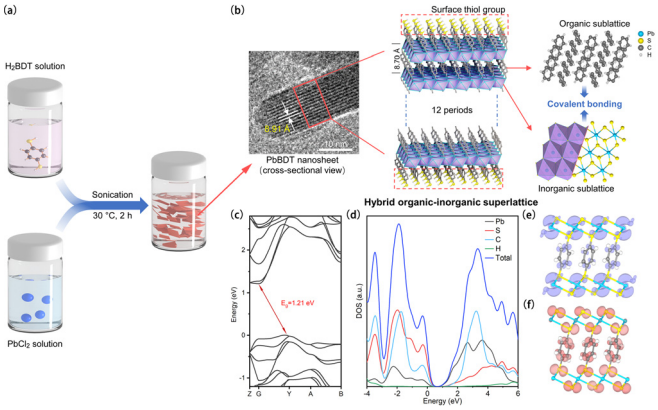

Figure 1. PbBDT OIHSL nanosheet: a) Fabrication of PbBDT nanosheets. b) Cross-section HRTEM image and crystal structure.[21] c) Calculated band structure and d) projected density of states (PDOS). e),f) Frontier electron density of CBM (e) and VBM (f).

six neighboring octahedra to form a layered [PbS_2] sublattice which resembles metastable 1T′-phase MoS_2.[16] [PbS_2] layers are further interconnected by benzene molecules via S–C covalent bond, which produces a clear superlattice alignment with periodically stacked inorganic and organic sublattices. Atomic force microscope (AFM) shows PbBDT nanosheets with a lateral dimension of 80 to 200 nm and a thickness of about 11 nm (Figure 2a). Cross-section high-resolution transmission electron microscope (HRTEM) image (Figure 1b) shows clear superlattice fringe with a space of 8.91 Å, which is close to the lattice distance (8.70 Å) of (002) plane. Interestingly, the surface of PbBDT nanosheets is covered with uncoordinated benzenethiol groups confirmed by Fourier transform infrared spectrum (Figure S8) and X-ray photoelectron spectroscopy (XPS) spectrum (Figure S9).[17] The phase purity of PbBDT nanosheets was verified by powder X-ray diffraction (PXRD) (Figure 2e) and elemental analysis (Table S1).

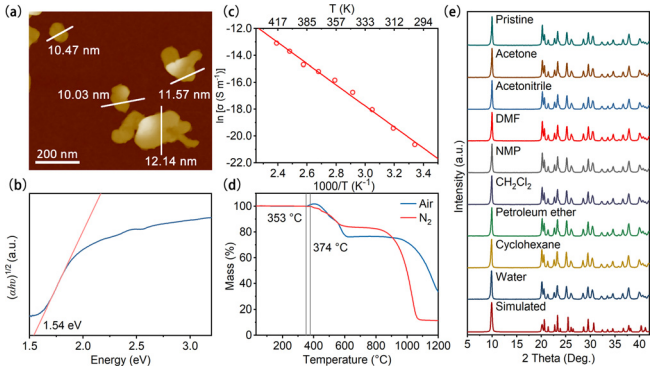

Figure 2. Basic characterizations of PbBDT OIHSL nanosheets: a) AFM image. b) Tauc plot. c) Fitting of conductivity–temperature data to Arrhenius equation. d) TG curve. e) PXRD patterns after immersion in different solvents for 24 h.

Density functional theory (DFT) calculation reveals a band gap of 1.21 eV, which is close to the estimated value (1.54 eV) from UV/Vis diffuse reflectance spectra (Figure 2b). Good linearity of lnσ to 1000/T (Figure 2c) confirmed the semiconductive nature of PbBDT. The conduction band minimum (CBM) (Figure 1c) exhibits a small dispersion of 0.03 eV along the inter-sublattice direction (G-Z), suggesting that electrons are mobile across layers (high symmetric points are defined in Figure S4). As shown in Figure 1d to f, the CBM of PbBDT arises predominately from the [PbS_2] sublattice with a decent contribution from the benzene sublattice while the valance band maximum (VBM) is mainly composed of S and C orbitals with a small contribution from Pb atoms. These results suggest better inter-sublattice electron transport compared with non-covalent OIHSLs.[11b,c] Moreover, covalent inter-sublattice connection endows PbBDT with higher thermal and chemical stability compared with non-covalent OIHSLs. PbBDT nanosheets are thermally stable up to 353 °C in air and 374 °C in N_2, respectively (Figure 2d) and remain intact after immersion in eight common solvents for 24 h (Figure 2e).

Surface functional groups and inter-sublattice electron coupling may endow PbBDT with fascinating performances in chemical applications. To verify this speculation, PbBDT nanosheet was employed as a chemiresistive gas-sensing material whose performance was evaluated using NO_2 as the molecule probe.

As shown in Figure 3d, the conductance of PbBDT showed a fast increase upon exposure to NO_2 and also a quick recovery after purging with air. PbBDT exhibited pronounced responses to a wide concentration range (40–4000 ppb) of NO_2 (Figure 3b). For comparison, we summarized the performances of reported NO_2 sensing materials with a response time <2 min and without light assistance (Figure 3f). Notably, PbBDT exhibited a very fast response (16.2 s for response, 47.4 s for recovery) to 400 ppb NO_2 (Figure 3d), while most room-temperature gas-sensing materials take more than 1 min to respond.[18c,i,19] PbBDT nanosheets showed an excellent sensitivity of 137.8 ppm^{-1} to 40 ppb NO_2, which is the highest value among the materials in Figure 3f. Theoretical limit of detection (LOD) was extrapolated from Figure 3c to be 0.51 ppb by setting the response as 0.1. This is the lowest record among all fast-response chemiresistive NO_2 sensing materials without light assistance. Owing to the selective interaction between thiol group and different molecules (details see DFT calculation in SI), PbBDT showed excellent selectivity to 13 typical interfering gases (Figure 3e). Besides, PbBDT also exhibited good long-

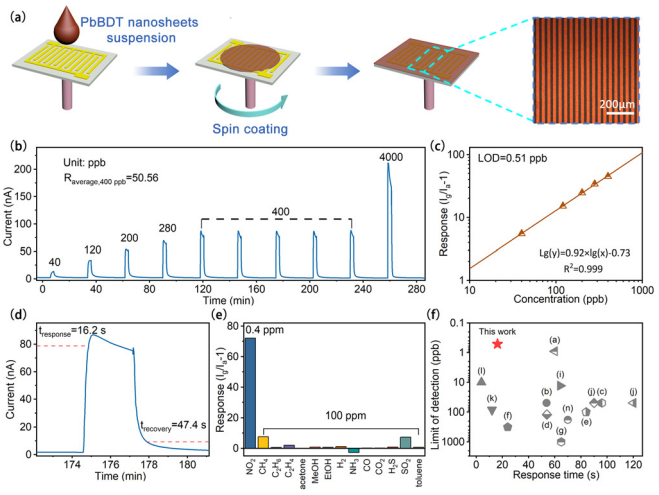

Figure 3. PbBDT OIHSL sensor: a) Fabrication processes and the photograph of the prepared sensor. b) Response and recovery curve towards NO_2 with different concentrations at room temperature. c) Log–log linear fitting of the response-concentration plot. d) Response and recovery time towards 400 ppb NO_2. e) Selectivity towards 13 interference gases. f) Reported fast-response NO_2 sensing materials.[18] Ag(SPh-NH_2),[18a] CuPc,[18b] $MnPS_3$,[18c] MoS_3 film,[18d] Te nanofibers,[18e] $LaFeO_3$ nanocubes,[18f] rGO/SnO_2,[18g] Au-impregnated WO_3 nanorods,[18h] In_2O_3,[18i] rGO/Co_3O_4,[18j] PbS CQDs,[18k] WS_2/ZnS,[18l] RGO/Fe_2O_3[18m] (data are obtained or estimated from the corresponding reports).

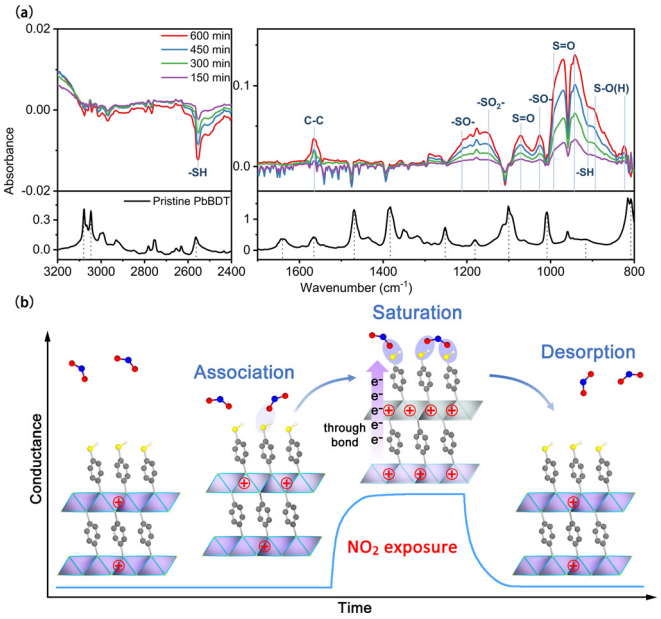

Figure 4. a) Time-resolved DRIFTS difference spectra of PbBDT during oxidation (colored) and spectrum of pristine PbBDT (black). b) The proposed sensing mechanism of PbBDT to NO_2.

term stability with 91.8% response retained after storage for 27 days (Figure S5).

The sensing response of PbBDT could be explained by its semiconductive nature and the strong interaction between NO_2 molecules and covalently anchored surface benzenethiol groups. NO_2 can easily adsorb onto PbBDT nanosheets through Lewis acid-base interaction and hydrogen bond with benzenethiol groups, wherein electrons can be extracted from PbBDT and transferred to NO_2 causing a resistivity change. To understand the role of the surface functional groups in gas sensing, we evaluated the performances of PbBDT nanosheets with different amounts of intact benzenethiol groups, which was controlled by in situ oxidation at 140 °C for different time (see SI). Time-resolved in situ diffuse reflectance infrared Fourier transform spectroscopy (DRIFTS) revealed the gradual oxidation of benzenethiol groups (Figure 4a). As oxidation time increased, -SH peaks (2559 and 916 cm^{-1}) were weakened while several new peaks ascribed to the oxidized products of benzenethiol groups (Table S4) appeared and were gradually enhanced. Meanwhile, the sensing performance of PbBDT was found to degenerate with oxidation time (Figure S6). These results suggest the sensing performance is directly correlated to the intact benzenethiol groups on PbBDT surface. Notably, no peak was found in the N 1s XPS spectra of PbBDT nanosheets after exposure to 100 ppm NO_2 for 12 h, suggesting reversible adsorption of NO_2 on the surface. Importantly, it is speculated that the inter-sublattice charge transport in PbBDT plays a fundamental role in transforming the surface disturbance into an electrical signal. When NO_2 adsorbs on the surface of PbBDT, owing to the covalent inter-sublattice connection, electrons across several layers may be extracted to create a relatively thick hole-accumulation layer (HAL), and a large change in carrier concentration can be observed (Figure 4b).[20] However, for OIHSLs with weak inter-sublattice interactions, the adsorption of analytes can only create a thin HAL, thereby leading to a limited conductance change.[18a]

In conclusion, aiming to overcome the challenge of preparing covalent single-crystal OIHSLs, a coordination assembly strategy was proposed. Accordingly, a single-crystal covalent OIHSL, PbBDT, was designed and prepared by a low-cost solution method. Different from the reported OIHSLs, organic and inorganic sublattices of PbBDT were covalently bonded along with electron coupling between them. Thanks to surface-decorated organic functional groups, such a covalent OIHSL with excellent thermo-/chemi-stability and inter-sublattice charge transport can enable superior chemistry applications. As a demonstration, the chemiresistive gas sensor based on PbBDT nanosheets shows the highest sensitivity, lowest LOD, very fast response and recovery, and excellent selectivity towards NO_2 at room temperature among all fast-response gas-sensing materials without light assistance. This work not only provides a feasible and general strategy for the preparation of single-crystal covalent OIHSLs but also demonstrates the potential of covalent OIHSLs in advanced chemical applications.

Acknowledgements

This work was supported by the NSF of China (21822109, 21975254, 21905280, 2020000052), the Key Research Program of Frontier Sciences, CAS (QYZDB-SSW-SLH023), the

Strategic Priority Research Program of CAS (XDB20000000), International Partnership Program of CAS (121835KYSB201800), China Postdoctoral Science Foundation (2019M662254), and Youth Innovation Promotion Association CAS. Fujian Science & Technology Innovation Laboratory for Optoelectronic Information of China (2021ZR101).

Conflict of Interest

The authors declare no conflict of interest.

Keywords: conductive coordination polymers · electrical devices · functional motifs · gas sensors · hybrid superlattice

[1] a) R. Ramesh, D. G. Schlom, *Nat. Rev. Mater.* **2019**, *4*, 257 – 268; b) D. Wu, A. Dehzangi, M. Razeghi, *Appl. Phys. Lett.* **2019**, *115*, 061102; c) D. Kazakov, M. Piccardo, Y. Wang, P. Chevalier, T. S. Mansuripur, F. Xie, C.-e. Zah, K. Lascola, A. Belyanin, F. Capasso, *Nat. Photonics* **2017**, *11*, 789 – 792.

[2] a) Y. Huang, J. Liang, C. Wang, S. Yin, W. Fu, H. Zhu, C. Wan, *Chem. Soc. Rev.* **2020**, *49*, 6866 – 6883; b) X. Qian, X. Gu, R. Yang, *Nano Energy* **2017**, *41*, 394 – 407; c) P. Xiong, Y. Wu, Y. Liu, R. Ma, T. Sasaki, X. Wang, J. Zhu, *Energy Environ. Sci.* **2020**, *13*, 4834 – 4853; d) P. Judeinstein, C. Sanchez, *J. Mater. Chem.* **1996**, *6*, 511 – 525; e) P. Rabu, M. Drillon, *Adv. Eng. Mater.* **2003**, *5*, 189 – 210.

[3] a) C. Wan, X. Gu, F. Dang, T. Itoh, Y. Wang, H. Sasaki, M. Kondo, K. Koga, K. Yabuki, G. J. Snyder, R. Yang, K. Koumoto, *Nat. Mater.* **2015**, *14*, 622 – 627; b) P. Xiong, R. Ma, N. Sakai, L. Nurdiwijayanto, T. Sasaki, *ACS Energy Lett.* **2018**, *3*, 997 – 1005; c) Z. Li, Y. Zhao, K. Mu, H. Shan, Y. Guo, J. Wu, Y. Su, Q. Wu, Z. Sun, A. Zhao, X. Cui, C. Wu, Y. Xie, *J. Am. Chem. Soc.* **2017**, *139*, 16398 – 16404.

[4] a) C. Zhang, J. Zhao, L. Zhou, Z. Li, M. Shao, M. Wei, *J. Mater. Chem. A* **2016**, *4*, 11516 – 11523; b) I. S. Kwon, I. H. Kwak, J. Y. Kim, H. G. Abbas, T. T. Debela, J. Seo, M. K. Cho, J. P. Ahn, J. Park, H. S. Kang, *Nanoscale* **2019**, *11*, 14266 – 14275; c) S. S. Wang, L. Jiao, Y. Qian, W. C. Hu, G. Y. Xu, C. Wang, H. L. Jiang, *Angew. Chem. Int. Ed.* **2019**, *58*, 10713 – 10717; *Angew. Chem.* **2019**, *131*, 10823 – 10827.

[5] N. Feng, R. Meng, L. Zu, Y. Feng, C. Peng, J. Huang, G. Liu, B. Chen, J. Yang, *Nat. Commun.* **2019**, *10*, 1372.

[6] P. P. Wang, H. Y. Li, H. Liu, P. He, B. Xu, X. Wang, *Small* **2015**, *11*, 3909 – 3915.

[7] a) M.-Y. Zhu, L.-X. Zhang, J. Yin, J.-J. Chen, L.-J. Bie, *Inorg. Chem. Front.* **2018**, *5*, 3046 – 3052; b) M.-Y. Zhu, L.-X. Zhang, J. Yin, J.-J. Chen, L.-J. Bie, B. D. Fahlman, *Sens. Actuators B* **2019**, *282*, 659 – 664.

[8] a) C. Wang, Q. He, U. Halim, Y. Liu, E. Zhu, Z. Lin, H. Xiao, X. Duan, Z. Feng, R. Cheng, N. O. Weiss, G. Ye, Y. C. Huang, H. Wu, H. C. Cheng, I. Shakir, L. Liao, X. Chen, W. A. Goddard III, Y. Huang, X. Duan, *Nature* **2018**, *555*, 231 – 236; b) A. Mal, R. K. Mishra, V. K. Praveen, M. A. Khayum, R. Banerjee, A. Ajayaghosh, *Angew. Chem. Int. Ed.* **2018**, *57*, 8443 – 8447; *Angew. Chem.* **2018**, *130*, 8579 – 8583.

[9] a) X. Y. Huang, J. Li, *J. Am. Chem. Soc.* **2007**, *129*, 3157 – 3162; b) J. Li, W. H. Bi, W. Ki, X. Y. Huang, S. Reddy, *J. Am. Chem. Soc.* **2007**, *129*, 14140 – 14141.

[10] a) B. Saparov, D. B. Mitzi, *Chem. Rev.* **2016**, *116*, 4558 – 4596; b) C. Katan, N. Mercier, J. Even, *Chem. Rev.* **2019**, *119*, 3140 – 3192.

[11] a) X. Zhang, M. Hejazi, S. J. Thiagarajan, W. R. Woerner, D. Banerjee, T. J. Emge, W. Xu, S. J. Teat, Q. Gong, A. Safari, R. Yang, J. B. Parise, J. Li, *J. Am. Chem. Soc.* **2013**, *135*, 17401 – 17407; b) D. Li, D. Li, H. Zhang, A. Yang, C. Liang, *J. Phys. Chem. Lett.* **2020**, *11*, 5282 – 5294; c) Z. Xiao, W. Meng, B. Saparov, H. S. Duan, C. Wang, C. Feng, W. Liao, W. Ke, D. Zhao, J. Wang, D. B. Mitzi, Y. Yan, *J. Phys. Chem. Lett.* **2016**, *7*, 1213 – 1218.

[12] a) J. Kim, C. T. T. Huong, N. V. Long, M. Yoon, M. J. Kim, J. K. Jeong, S. Choi, D. H. Kim, C. H. Lee, S. U. Lee, M. M. Sung, *Nano Lett.* **2020**, *20*, 4864 – 4871; b) A. Giri, J.-P. Niemelä, C. J. Szwejkowski, M. Karppinen, P. E. Hopkins, *Phys. Rev. B* **2016**, *93*, 024201.

[13] a) B. Yoon, B. H. Lee, S. M. George, *ECS Trans.* **2011**, *41*, 271 – 277; b) B. H. Lee, B. Yoon, A. I. Abdulagatov, R. A. Hall, S. M. George, *Adv. Funct. Mater.* **2013**, *23*, 532 – 546.

[14] a) H. Furukawa, K. E. Cordova, M. O'Keeffe, O. M. Yaghi, *Science* **2013**, *341*, 1230444; b) L. Jiao, Y. Wang, H. L. Jiang, Q. Xu, *Adv. Mater.* **2018**, *30*, 1703663; c) Y. Li, J. Huang, Z.-W. Mo, X.-W. Zhang, X.-N. Cheng, L. Gong, D.-D. Zhou, J.-P. Zhang, *Sci. Bull.* **2019**, *64*, 964 – 967; d) G. Das, B. P. Biswal, S. Kandambeth, V. Venkatesh, G. Kaur, M. Addicoat, T. Heine, S. Verma, R. Banerjee, *Chem. Sci.* **2015**, *6*, 3931 – 3939.

[15] a) T. D. Bennett, S. Horike, *Nat. Rev. Mater.* **2018**, *3*, 431 – 440; b) S. Sakaida, K. Otsubo, O. Sakata, C. Song, A. Fujiwara, M. Takata, H. Kitagawa, *Nat. Chem.* **2016**, *8*, 377 – 383.

[16] Z. Lai, Q. He, T. H. Tran, D. V. M. Repaka, D. D. Zhou, Y. Sun, S. Xi, Y. Li, A. Chaturvedi, C. Tan, B. Chen, G. H. Nam, B. Li, C. Ling, W. Zhai, Z. Shi, D. Hu, V. Sharma, Z. Hu, Y. Chen, Z. Zhang, Y. Yu, X. Renshaw Wang, R. V. Ramanujan, Y. Ma, K. Hippalgaonkar, H. Zhang, *Nat. Mater.* **2021**, https://doi.org/10.1038/s41563-41021-00971-y.

[17] a) X. Meng, E. Kolodzeiski, X. Huang, A. Timmer, B. Schulze Lammers, H. Y. Gao, H. Mönig, L. Liu, W. Xu, S. Amirjalayer, D. Zhu, H. Fuchs, *ChemNanoMat* **2020**, *6*, 1479 – 1484; b) V. B. Engelkes, J. M. Beebe, C. D. Frisbie, *J. Am. Chem. Soc.* **2004**, *126*, 14287 – 14296.

[18] a) H. Jiang, L. Cao, Y. Li, W. Li, X. Ye, W. Deng, X. Jiang, G. Wang, G. Xu, *Chem. Commun.* **2020**, *56*, 5366 – 5369; b) L. S. Chia, Y. H. Du, S. Palale, P. S. Lee, *ACS Omega* **2019**, *4*, 10388 – 10395; c) R. Kumar, R. N. Jenjeti, S. Sampath, *ACS Sens.* **2020**, *5*, 404 – 411; d) B. Cho, A. R. Kim, Y. Park, J. Yoon, Y. J. Lee, S. Lee, T. J. Yoo, C. G. Kang, B. H. Lee, H. C. Ko, D. H. Kim, M. G. Hahm, *ACS Appl. Mater. Interfaces* **2015**, *7*, 2952 – 2959; e) H. Park, H. Jung, M. Zhang, C. H. Chang, N. G. Ndifor-Angwafor, Y. Choa, N. V. Myung, *Nanoscale* **2013**, *5*, 3058 – 3062; f) S. Thirumalairajan, K. Girija, V. R. Mastelaro, N. Ponpandian, *ACS Appl. Mater. Interfaces* **2014**, *6*, 13917 – 13927; g) S. Mao, S. Cui, G. Lu, K. Yu, Z. Wen, J. Chen, *J. Mater. Chem.* **2012**, *22*, 11009 – 11013; h) S. Kabcum, N. Kotchasak, D. Channei, A. Tuantranont, A. Wisitsoraat, S. Phanichphant, C. Liewhiran, *Sens. Actuators B* **2017**, *252*, 523 – 536; i) Y. Ren, X. Zhou, W. Luo, P. Xu, Y. Zhu, X. Li, X. Cheng, Y. Deng, D. Zhao, *Chem. Mater.* **2016**, *28*, 7997 – 8005; j) B. Zhang, M. Cheng, G. Liu, Y. Gao, L. Zhao, S. Li, Y. Wang, F. Liu, X. Liang, T. Zhang, G. Lu, *Sens. Actuators B* **2018**, *263*, 387 – 399; k) H. Liu, M. Li, O. Voznyy, L. Hu, Q. Fu, D. Zhou, Z. Xia, E. H. Sargent, J. Tang, *Adv. Mater.* **2014**, *26*, 2718 – 2724; l) Y. Han, Y. Liu, C. Su, S. Wang, H. Li, M. Zeng, N. Hu, Y. Su, Z. Zhou, H. Wei, Z. Yang, *Sens. Actuators B* **2019**, *296*, 126666; m) Y.-l. Dong, X.-f. Zhang, X.-l. Cheng, Y.-m. Xu, S. Gao, H. Zhao, L.-h. Huo, *RSC Adv.* **2014**, *4*, 57493 – 57500.

[19] a) J. Zhou, X. F. Cheng, B. J. Gao, C. Yu, J. H. He, Q. F. Xu, H. Li, N. J. Li, D. Y. Chen, J. M. Lu, *Small* **2019**, *15*, 1803896; b) C. Yu, H.-Z. Lin, J. Zhou, X.-F. Cheng, J.-H. He, H. Li, Q.-F. Xu, N.-J. Li, D.-Y. Chen, J.-M. Lu, *J. Mater. Chem. A* **2020**, *8*, 1052 – 1058; c) J. Lu, D. Liu, J. Zhou, Y. Chu, Y. Chen, X. Wu, J. Huang, *Adv. Funct. Mater.* **2017**, *27*, 1700018.

[20] a) H.-J. Kim, J.-H. Lee, *Sens. Actuators B* **2014**, *192*, 607 – 627; b) M. H. Raza, K. Movlaee, S. G. Leonardi, N. Barsan, G. Neri, N. Pinna, *Adv. Funct. Mater.* **2020**, *30*, 1906874.

[21] Deposition Number 2084844 contains the supplementary crystallographic data for this paper. These data are provided free of charge by the joint Cambridge Crystallographic Data Centre and Fachinformationszentrum Karlsruhe Access Structures service www.ccdc.cam.ac.uk/structures.

Manuscript received: May 29, 2021
Revised manuscript received: June 29, 2021
Accepted manuscript online: July 9, 2021
Version of record online: August 6, 2021

